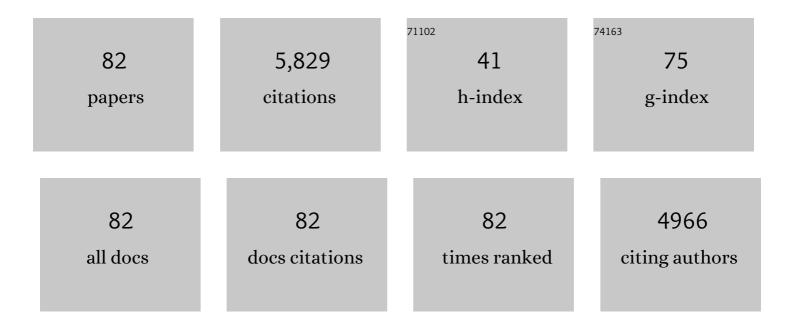
Lorenz Holzer

List of Publications by Year in descending order

Source: https://exaly.com/author-pdf/4087007/publications.pdf Version: 2024-02-01



#	Article	IF	CITATIONS
1	Anodic degradation of Zn-Ni coatings in moderately alkaline NaCl solution. Materials Letters, 2021, 293, 129701.	2.6	8
2	Microstructural aspects of Ti6Al4V degradation in H2O2-containing phosphate buffered saline. Corrosion Science, 2021, 190, 109640.	6.6	25
3	Modeling the impedance response and steady state behaviour of porous CGO-based MIEC anodes. Physical Chemistry Chemical Physics, 2021, 23, 23042-23074.	2.8	6
4	Quantifying the influence of microstructure on effective conductivity and permeability: Virtual materials testing. International Journal of Solids and Structures, 2020, 184, 211-220.	2.7	48
5	Impedance Spectroscopy Analysis of Structural Defects in Sputtered ZnO Films. ChemElectroChem, 2020, 7, 2055-2064.	3.4	5
6	Oxygen Reduction Investigation on Sputtered ZnO Layers with Nanoâ \in granular Structure. ChemElectroChem, 2019, 6, 5321-5330.	3.4	4
7	Estimating the effective elasticity properties of a diamond/ \hat{l}^2 -SiC composite thin film by 3D reconstruction and numerical homogenization. Diamond and Related Materials, 2019, 97, 107406.	3.9	6
8	Stochastic 3D Modeling of Three-Phase Microstructures for Predicting Transport Properties: A Case Study. Transport in Porous Media, 2019, 128, 179-200.	2.6	10
9	Sulfur Poisoning Recovery on a Solid Oxide Fuel Cell Anode Material through Reversible Segregation of Nickel. Chemistry of Materials, 2019, 31, 748-758.	6.7	36
10	Imageâ€Based Upscaling of Permeability in Opalinus Clay. Journal of Geophysical Research: Solid Earth, 2018, 123, 285-295.	3.4	32
11	Cathodic Corrosion of Zinc under Potentiostatic Conditions in NaCl Solutions. ChemElectroChem, 2018, 5, 1203-1211.	3.4	10
12	An Ensemble Monte Carlo Simulation Study of Water Distribution in Porous Gas Diffusion Layers for Proton Exchange Membrane Fuel Cells. Journal of Electrochemical Energy Conversion and Storage, 2018, 15, .	2.1	3
13	Lanthanum doped strontium titanate - ceria anodes: deconvolution of impedance spectra and relationship with composition and microstructure. Journal of Power Sources, 2018, 385, 62-75.	7.8	18
14	On Microstructure-Property Relationships Derived by Virtual Materials Testing with an Emphasis on Effective Conductivity. Communications in Computer and Information Science, 2018, , 145-158.	0.5	0
15	Microstructure-property relationships in a gas diffusion layer (GDL) for Polymer Electrolyte Fuel Cells, Part I: effect of compression and anisotropy of dry GDL. Electrochimica Acta, 2017, 227, 419-434.	5.2	74
16	Big data for microstructureâ€property relationships: A case study of predicting effective conductivities. AICHE Journal, 2017, 63, 4224-4232.	3.6	32
17	Microstructure-property relationships in a gas diffusion layer (GDL) for Polymer Electrolyte Fuel Cells, Part II: pressure-induced water injection and liquid permeability. Electrochimica Acta, 2017, 241, 414-432.	5.2	26
18	Microstructure and spatial distribution of corrosion products anodically grown on zinc in chloride solutions. Electrochemistry Communications, 2017, 81, 56-60.	4.7	22

#	Article	IF	CITATIONS
19	Structural Reversibility and Nickel Particle stability in Lanthanum Iron Nickel Perovskiteâ€Type Catalysts. ChemSusChem, 2017, 10, 2505-2517.	6.8	52
20	A FIB-nanotomography method for accurate 3D reconstruction of open nanoporous structures. Ultramicroscopy, 2016, 163, 38-47.	1.9	50
21	Fundamental relationships between 3D pore topology, electrolyte conduction and flow properties: Towards knowledge-based design of ceramic diaphragms for sensor applications. Materials and Design, 2016, 99, 314-327.	7.0	19
22	Development of improved nickel catalysts for sorption enhanced CO2 methanation. International Journal of Hydrogen Energy, 2016, 41, 20185-20191.	7.1	64
23	Smart material concept: reversible microstructural self-regeneration for catalytic applications. Journal of Materials Chemistry A, 2016, 4, 11939-11948.	10.3	72
24	Stochastic 3D modeling of complex three-phase microstructures in SOFC-electrodes with completely connected phases. Computational Materials Science, 2016, 118, 353-364.	3.0	33
25	Predicting effective conductivities based on geometric microstructure characteristics. AICHE Journal, 2016, 62, 1834-1843.	3.6	87
26	3D Microstructure Effects in Ni-YSZ Anodes: Prediction of Effective Transport Properties and Optimization of Redox Stability. Materials, 2015, 8, 5554-5585.	2.9	40
27	3D Microstructure Effects in Ni-YSZ Anodes: Influence of TPB Lengths on the Electrochemical Performance. Materials, 2015, 8, 7129-7144.	2.9	26
28	Ohmic resistance of nickel infiltrated chromium oxide scales in solid oxide fuel cell metallic interconnects. Solid State Ionics, 2015, 283, 38-51.	2.7	4
29	A model-based approach for current voltage analyses to quantify degradation and fuel distribution in solid oxide fuel cell stacks. Journal of Power Sources, 2015, 288, 409-418.	7.8	12
30	Intergranular pore space evolution in MX80 bentonite during a long-term experiment. Applied Clay Science, 2015, 104, 150-159.	5.2	8
31	Influence of strontium-rich pore-filling phase on the performance of La0.6Sr0.4CoO3â^' thin-film cathodes. Journal of Power Sources, 2015, 274, 295-303.	7.8	9
32	The Pore Structure of Compacted and Partly Saturated MX-80 Bentonite at Different Dry Densities. Clays and Clay Minerals, 2014, 62, 174-187.	1.3	24
33	Advances in 3D focused ion beam tomography. MRS Bulletin, 2014, 39, 354-360.	3.5	69
34	Model-based prediction of the ohmic resistance of metallic interconnects from oxide scale growth based on scanning electron microscopy. Journal of Power Sources, 2014, 272, 595-605.	7.8	14
35	Quantitative relationships between microstructure and effective transport properties based on virtual materials testing. AICHE Journal, 2014, 60, 1983-1999.	3.6	82
36	Characterization of multi-scale microstructural features in Opalinus Clay. Microporous and Mesoporous Materials, 2013, 170, 83-94.	4.4	152

#	Article	IF	CITATIONS
37	Cr 2 O 3 scale growth rates on metallic interconnectors derived from 40,000Âh solid oxide fuel cell stack operation. Journal of Power Sources, 2013, 243, 508-518.	7.8	38
38	The influence of constrictivity on the effective transport properties of porous layers in electrolysis and fuel cells. Journal of Materials Science, 2013, 48, 2934-2952.	3.7	128
39	Threeâ€ d imensional pore structure and ion conductivity of porous ceramic diaphragms. AICHE Journal, 2013, 59, 1446-1457.	3.6	52
40	Redox cycling of Ni–YSZ anodes for solid oxide fuel cells: Influence of tortuosity, constriction and percolation factors on the effective transport properties. Journal of Power Sources, 2013, 242, 179-194.	7.8	59
41	Stochastic 3D modeling of La0.6Sr0.4CoO3â^î^ cathodes based on structural segmentation of FIB–SEM images. Computational Materials Science, 2013, 67, 48-62.	3.0	38
42	Pore space relevant for gas permeability in Opalinus clay: Statistical analysis of homogeneity, percolation, and representative volume element. Journal of Geophysical Research: Solid Earth, 2013, 118, 2799-2812.	3.4	91
43	A computational study of the effect of structural anisotropy of porous asphalt on hydraulic conductivity. Construction and Building Materials, 2012, 36, 66-77.	7.2	39
44	On the chemical interaction of nanoscale lanthanum doped strontium titanates with common scandium and yttrium stabilized electrolyte materials. International Journal of Hydrogen Energy, 2012, 37, 18326-18341.	7.1	14
45	Synthesis and performance of A-site deficient lanthanum-doped strontium titanate by nanoparticle based spray pyrolysis. Journal of Power Sources, 2012, 201, 26-36.	7.8	55
46	Nickel agglomeration in solid oxide fuel cells: The influence of temperature. Solid State Ionics, 2012, 211, 69-73.	2.7	45
47	3D geometry and topology of pore pathways in Opalinus clay: Implications for mass transport. Applied Clay Science, 2011, 52, 85-95.	5.2	190
48	On the application of focused ion beam nanotomography in characterizing the 3D pore space geometry of Opalinus clay. Physics and Chemistry of the Earth, 2011, 36, 1539-1544.	2.9	75
49	Quantitative relationships between composition, particle size, triple phase boundary length and surface area in nickel-cermet anodes for Solid Oxide Fuel Cells. Journal of Power Sources, 2011, 196, 7076-7089.	7.8	131
50	Microstructure degradation of cermet anodes for solid oxide fuel cells: Quantification of nickel grain growth in dry and in humid atmospheres. Journal of Power Sources, 2011, 196, 1279-1294.	7.8	255
51	Nanoscale calcium bismuth mixed oxide with enhanced photocatalytic performance under visible light. Applied Catalysis A: General, 2010, 382, 190-196.	4.3	8
52	Effect of graphite pore former on oxygen electrodes prepared with La0.6Sr0.4CoO3â^' nanoparticles. Electrochemistry Communications, 2010, 12, 292-295.	4.7	33
53	Shape Comparison between 0.4–2.0 and 20–60 μm Cement Particles. Journal of the American Ceramic Society, 2010, 93, 1626-1633.	3.8	27
54	3D-microstructure analysis of hydrated bentonite with cryo-stabilized pore water. Applied Clay Science, 2010, 47, 330-342.	5.2	84

#	Article	IF	CITATIONS
55	Influence of Some Inorganic Impurities on the Electrochemical Properties and Microstructure of Ni-CGO Anode in Artificial Woodgas Atmosphere. ECS Transactions, 2009, 25, 2117-2124.	0.5	0
56	Interaction of polycarboxylate-based superplasticizers with cements containing different C3A amounts. Cement and Concrete Composites, 2009, 31, 153-162.	10.7	255
57	Toward Reproducible Three-Dimensional Microstructure Analysis of Granular Materials and Complex Suspensions. Microscopy and Microanalysis, 2009, 15, 130-146.	0.4	20
58	Adsorption of polyelectrolytes and its influence on the rheology, zeta potential, and microstructure of various cement and hydrate phases. Journal of Colloid and Interface Science, 2008, 323, 301-312.	9.4	314
59	The microstructure of dispersed and non-dispersed fresh cement pastes — New insight by cryo-microscopy. Cement and Concrete Research, 2008, 38, 522-529.	11.0	117
60	Contradicting Geometrical Concepts in Pore Size Analysis Attained with Electron Microscopy and Mercury Intrusion. Journal of the American Ceramic Society, 2008, 91, 4059-4067.	3.8	338
61	Limitation in obtainable surface roughness of hardened cement paste: â€`virtual' topographic experiment based on focussed ion beam nanotomography datasets. Journal of Microscopy, 2008, 232, 200-206.	1.8	27
62	Three-Dimensional Microstructural Characterization Using Focused Ion Beam Tomography. MRS Bulletin, 2007, 32, 408-416.	3.5	190
63	In situ nanomanipulators as a tool to separate individual tobermorite crystals for AFM studies. Ultramicroscopy, 2007, 107, 1068-1077.	1.9	5
64	Cryoâ€FIBâ€nanotomography for quantitative analysis of particle structures in cement suspensions. Journal of Microscopy, 2007, 227, 216-228.	1.8	54
65	Hydration of alkali-activated slag: comparison with ordinary Portland cement. Advances in Cement Research, 2006, 18, 119-128.	1.6	256
66	FIB-Nanotomography of Particulate Systems—Part I: Particle Shape and Topology of Interfaces. Journal of the American Ceramic Society, 2006, 89, 2577-2585.	3.8	125
67	FIB-Nanotomography of Particulate Systems—Part II: Particle Recognition and Effect of Boundary Truncation. Journal of the American Ceramic Society, 2006, 89, 2586-2595.	3.8	73
68	Changes in microstructures and physical properties of polymer-modified mortars during wet storage. Cement and Concrete Research, 2006, 36, 79-90.	11.0	101
69	Influence of compaction on the interfacial transition zone and the permeability of concrete. Cement and Concrete Research, 2006, 36, 1425-1433.	11.0	116
70	QUANTIFICATION OF CAPILLARY PORES AND HADLEY GRAINS IN CEMENT PASTE USING FIB-NANOTOMOGRAPHY. , 2006, , 509-516.		8
71	Influence of polymers on microstructure and adhesive strength of cementitious tile adhesive mortars. Cement and Concrete Research, 2005, 35, 35-50.	11.0	196
72	Alkali-aggregate reaction—identifying reactive silicates in complex aggregates by ESEM observation of dissolution features. Cement and Concrete Composites, 2005, 27, 796-801.	10.7	28

#	Article	IF	CITATIONS
73	Three-dimensional analysis of porous BaTiO3 ceramics using FIB nanotomography. Journal of Microscopy, 2004, 216, 84-95.	1.8	324
74	Transfer of a single particle for combined ESEM and TEM analyses. Atmospheric Environment, 2003, 37, 4353-4359.	4.1	14
75	Quantitative microstructure analysis of polymer-modified mortars. Journal of Microscopy, 2003, 212, 186-196.	1.8	33
76	Swiss tunnel structures: concrete damage by formation of thaumasite. Cement and Concrete Composites, 2003, 25, 1111-1117.	10.7	67
77	Geochronology of the Hout River Shear Zone and the metamorphism in the Southern Marginal Zone of the Limpopo Belt, Southern Africa. Precambrian Research, 2001, 109, 145-173.	2.7	123
78	The behaviour of Nd and Pb isotopes during 2.0 Ga migmatization in paragneisses of the Central Zone of the Limpopo Belt (South Africa and Botswana). Precambrian Research, 2001, 112, 51-86.	2.7	44
79	Tectonothermal history of the western part of the Limpopo Belt: tectonic models and new perspectives. Journal of African Earth Sciences, 1999, 28, 383-402.	2.0	105
80	Exhumation of Limpopo Central Zone granulites and dextral continent-scale transcurrent movement at 2.0 Ga along the Palala Shear Zone, Northern Province, South Africa. Precambrian Research, 1999, 96, 263-288.	2.7	88
81	Unraveling the record of successive high grade events in the Central Zone of the Limpopo Belt using Pb single phase dating of metamorphic minerals. Precambrian Research, 1998, 87, 87-115.	2.7	171
82	Discrete metamorphic events in the Limpopo belt, southern Africa: Implications for the application of P-T paths in complex metamorphic terrains. Geology, 1994, 22, 1035.	4.4	93